Intrinsic electron traps in atomic-layer deposited HfO2 insulators

F. Cerbu, O. Madia, D. V. Andreev, S. Fadida, M. Eizenberg, L. Breuil, J. G. Lisoni, J. A. Kittl, J. Strand, A. L. Shluger, V. V. Afanas'ev, M. Houssa, and A. Stesmans

Citation: Applied Physics Letters **108**, 222901 (2016); doi: 10.1063/1.4952718
View online: http://dx.doi.org/10.1063/1.4952718
View Table of Contents: http://scitation.aip.org/content/aip/journal/apl/108/22?ver=pdfcov
Published by the AIP Publishing

Articles you may be interested in

Spectroscopic investigation of the electronic structure of thin atomic layer deposition HfO2 films
J. Vac. Sci. Technol. A **34**, 01A117 (2016); 10.1116/1.4935338

Low-temperature plasma-enhanced atomic layer deposition of HfO2/Al2O3 nanolaminate structure on Si
J. Vac. Sci. Technol. B **33**, 01A101 (2015); 10.1116/1.4895010

Surface band bending and band alignment of plasma enhanced atomic layer deposited dielectrics on Ga- and N-face gallium nitride
J. Appl. Phys. **116**, 123702 (2014); 10.1063/1.4895985

Energy band alignment of atomic layer deposited HfO2 oxide film on epitaxial (100)Ge, (110)Ge, and (111)Ge layers
J. Appl. Phys. **113**, 114303 (2013); 10.1063/1.4795284

Band offset determination of atomic-layer-deposited Al2O3 and HfO2 on InP by internal photoemission and spectroscopic ellipsometry
J. Appl. Phys. **113**, 024504 (2013); 10.1063/1.4774038

AIP Applied Physics Reviews
NEW Special Topic Sections
NOW ONLINE
Lithium Niobate Properties and Applications: Reviews of Emerging Trends
AIP Applied Physics Reviews

Reuse of AIP Publishing content is subject to the terms at: https://publishing.aip.org/authors/rights-and-permissions. Download to IP: 128.40.8.138 On: Tue, 31 May 2016 17:14:45

APPLIED PHYSICS LETTERS **108**, 222901 (2016)

Intrinsic electron traps in atomic-layer deposited HfO_2 insulators

F. Cerbu,[1] O. Madia,[1] D. V. Andreev,[1,2] S. Fadida,[3] M. Eizenberg,[3] L. Breuil,[4] J. G. Lisoni,[4,5] J. A. Kittl,[1,6] J. Strand,[7] A. L. Shluger,[7] V. V. Afanas'ev,[1] M. Houssa,[1] and A. Stesmans[1]
[1]*Laboratory of Semiconductor Physics, Department of Physics and Astronomy, University of Leuven, 3001 Leuven, Belgium*
[2]*Bauman Moscow State Technical University—Kaluga Branch, 248000 Kaluga, Moscow obl., Russian Federation*
[3]*Department of Materials Science and Engineering, Technion-Israel Institute of Technology, 32000 Haifa, Israel*
[4]*imec, 3001 Leuven, Belgium*
[5]*Institute of Physics and Mathematics, Faculty of Science, Universidad Austral de Chile, Valdivia, Chile*
[6]*Advanced Logic Lab, Samsung Semiconductor, Inc., Austin, 78754 Texas, USA*
[7]*Department of Physics and Astronomy, University College London, London WC1E 6BT, United Kingdom*

(Received 2 February 2016; accepted 14 May 2016; published online 31 May 2016)

Analysis of photodepopulation of electron traps in HfO_2 films grown by atomic layer deposition is shown to provide the trap energy distribution across the entire oxide bandgap. The presence is revealed of two kinds of deep electron traps energetically distributed at around $E_t \approx 2.0$ eV and $E_t \approx 3.0$ eV below the oxide conduction band. Comparison of the trapped electron energy distributions in HfO_2 layers prepared using different precursors or subjected to thermal treatment suggests that these centers are intrinsic in origin. However, the common assumption that these would implicate O vacancies cannot explain the charging behavior of HfO_2, suggesting that alternative defect models should be considered. *Published by AIP Publishing.* [http://dx.doi.org/10.1063/1.4952718]

In recent years, hafnium dioxide (HfO_2) based insulators have emerged as the primary contenders to replace traditional SiO_2 in a variety of nano-electronic devices ranging from deep-scaled transistors to DRAM[1,2] and non-volatile memory cells.[3,4] Furthermore, thanks to the ferroelectricity property of both doped[5,6] and pure[7] HfO_2, novel applications including memories[8] and high sub-threshold slope transistors[9] are envisioned. However, the reliability of the dielectric associated with electron trapping appears to be the "show stopper": It has already been shown that the positive bias-temperature instability (PBTI) limits the gate oxide scaling in metal-HfO_2-Si transistors[10–13] while in flash cells, electron trapping in the inter-gate HfO_2 insulator degrades the program/erase window, retention, and endurance.[14,15] Moreover, in ferroelectric applications, trapping of electrons within HfO_2 will screen the electric field at the surface of the semiconductor channel, thus directly impairing the device functionality. In particular, electron injection and trapping are expected to be an issue because of the high coercive field strength typical for ferroelectric HfO_2.[16] This signifies the importance of developing proper methods for quantifying and analyzing electron traps aiming at their atomic identification to eventually allow one to eliminate or limit their detrimental impact.

Yet, despite numerous indications of electron traps in HfO_2, little is still known about their atomic origin and the distribution of energy levels. Electron traps in HfO_2 are often associated with oxygen vacancy defects[10] on the basis of electron energy levels found in the energy range 1.2–1.8 eV below the conduction band (CB) bottom edge.[10,14] However, since theoretical calculations consistently predict that the O vacancy in HfO_2 can act also as a hole trap,[17–21] this assignment cannot be reconciled with the absence of hole trapping from the valence band (VB) inside the high-k layer:[22] The observed trapped hole charge in the SiO_2/HfO_2 stacks appears to be insensitive to the HfO_2 layer thickness ranging from 5 to >100 nm. Rather, the strong electron trapping in HfO_2 films prepared from the nitrato precursor $Hf(NO_3)_4$ can be correlated with the presence of N-related defects revealed by electron spin resonance (ESR)[22,23] suggesting an impurity-related electron trapping. Since then, numerous ESR experiments on the production-grade HfO_2 layers have failed to reveal any feasible signal, prompting the search for alternative trap characterization method(s).

In the present work, we demonstrate that the exhaustive photo-depopulation spectroscopy (EPDS) allows one to determine the energy distribution of trapped electrons in the HfO_2 bandgap. Studies on HfO_2 layers prepared using three different production-grade atomic layer deposition (ALD) routes have demonstrated that at least two different components in the electron trap spectrum are sensitive both to the deposition chemistry and to the subsequent thermal processing. On the basis of these observations, we argue that these traps are associated with intrinsic defects in HfO_2, sensitive to the HfO_2 phase [amorphous (a-) vs. crystalline]. However, upon re-evaluation of the energy levels pertaining to the O vacancy in a-hafnia, we conclude that this model cannot account for the revealed charging behavior and that alternative atomic configurations are at the origin of the electron trapping sites.

Samples were prepared by ALD of 19–20 nm thick HfO_2 on a 5- or 7.5-nm thick SiO_2 layer thermally grown on (100)Si substrates. This SiO_2 layer serves as the tunnel oxide enabling electron injection from Si into the HfO_2 films prepared using three production-grade ALD processes, labeled as A, B, and C: A—using $HfCl_4 + H_2O$ precursors at 300 °C; B—using tetrakis(dimethylamido)hafnium (TDMA-Hf) and H_2O at 300 °C; C—state-of-the-art industrial Cl-free ALD process. For the sake of comparison, process A was also used to synthesize 19-nm thick $Hf_{0.8}Al_{0.2}O_x$ (20 at. % Al nominal)

Reuse of AIP Publishing content is subject to the terms at: https://publishing.aip.org/authors/rights-and-permissions. Download to IP: 128.40.8.138 On: Tue, 31 May 2016 17:14:45

layers by combining $HfCl_4$ and $Al(CH_3)_3$ pulses. In addition to the as-deposited films, samples annealed for 15 min in N_2 (1 atm) at 600, 800, or 1000 °C were also analyzed. Metal-oxide-Si (MOS) capacitors were completed by thermoresistive evaporation of semitransparent electrodes (13 nm Au) of 1 mm^2 area. Alternatively, 10 nm TiN/2 nm Si electrodes were formed by physical vapor deposition followed by a 30 min anneal in forming gas (10%H_2 + N_2) at 400 °C.

The EPDS, carried out under application of small positive metal bias (+1 or +2 V), allows the photo-depopulation of electron states in the oxide to reach saturation at a given photon energy $h\nu$ and quantifies the corresponding charge variation from the observed capacitance-voltage (CV) curve shift.[24–26] The saturation of de-trapping means that all charge carriers available for photo-excitation at this $h\nu$ value are removed (the charge reservoir is exhausted), i.e., there are no electrons left in the states with the optical energy depth $E_t < h\nu$ below the CB bottom. On starting the illumination from a low photon energy $h\nu$ and then, after having reached saturation, increasing $h\nu$ by a small energy step $\delta h\nu$, the next saturation of the de-trapping kinetics would correspond to the complete removal of charge carriers from the traps in the energy interval $\{h\nu; h\nu + \delta h\nu\}$. Then, by performing the depopulation at incremental photon energies, one can find the distribution of the electron states as a function of E_t across the insulator bandgap. Importantly, unlike in the photocurrent measurements, charge monitoring allows the determination of its sign thus enabling discrimination between the excitation of an electron from the insulator valence band (VB) to the empty defect level (negative charging) or the removal of an electron from the gap state to the CB (positive charging). The remaining task consists in the separation of donor and acceptor states corresponding to (0/+ or +/0) and (0/− or −/0) transitions, respectively. The latter is achieved by correlating the density of states inferred from EPDS to the initial net charge in the insulating stack. This charge can be controllably varied by injecting electrons or holes from the Si substrate (tunnelling through the SiO_2 barrier) or e-h pair generation in the insulator under UV illumination through the semitransparent metal gate.[22,24] Technical details of the measurements are summarized in the supplementary material.[27]

Figure 1 compares the illumination-induced charge Q_{stack} variation (a), (b) and the of these derived spectral charge density (SCD) (c), (d) spectra in the pristine and electron-injected (charging voltage pulse $V_g = +15$ V applied to the metal electrode) samples with 19-nm thick HfO_2 and $Hf_{0.8}Al_{0.2}O_x$ insulators (panels a/c and b/d, respectively) fabricated using the $HfCl_4$-based process A. One can distinguish three spectral ranges with different electron transitions dominating the charging process. First, for $h\nu < 4$ eV, electrons are excited from the energy levels in the oxide gap [cf. transition 1 in the inset in Fig. 1(a)] leading to a slight "positive" charging in the pristine HfO_2 film or, else, to the removal of electrons captured in the HfO_2 or $Hf_{0.8}Al_{0.2}O_x$ layer upon electron tunnelling. Two important features are worth noting: (1) in the electron-injected samples, all the trapped electrons can be de-trapped under illumination in the spectral range $h\nu < 4$ eV; (2) the charging spectrum of the pristine HfO_2 layer fits in with that of the electron de-trapping suggesting that the "positive" charging of the as-deposited HfO_2 layer is also due to the de-trapping of electrons from part of the acceptor states filled by electrons during ALD.

Second, when $h\nu$ exceeds 4 eV, the sign of the charging changes to negative. The same effect has been observed earlier in SiO_2/Y_2O_3[25] and SiO_2/Al_2O_3 stacks.[26] It is related to photo-injection of electrons from Si into the SiO_2 barrier layer and the subsequent trapping of these in HfO_2 [cf. transition 2 in Fig. 1(a)]. The saturation negative charge density detected in the EPDS corresponds to the balance between the trapping of the electrons photo-injected from Si and their de-trapping by the optical transitions of type 1. Third and finally, when $h\nu$ reaches the threshold of intrinsic photoconductivity of HfO_2 (the lowest bandgap $E_g = 5.6$ eV corresponds to the monoclinic phase, see Ref. 28), the generation of electron-hole pairs within the HfO_2 layer leads to the annihilation of trapped electrons.[22] Since the final charge state of the oxide stack after exposure to photons with $h\nu > 5.6$ eV is indistinguishable from that of the as-prepared (neutral) oxide

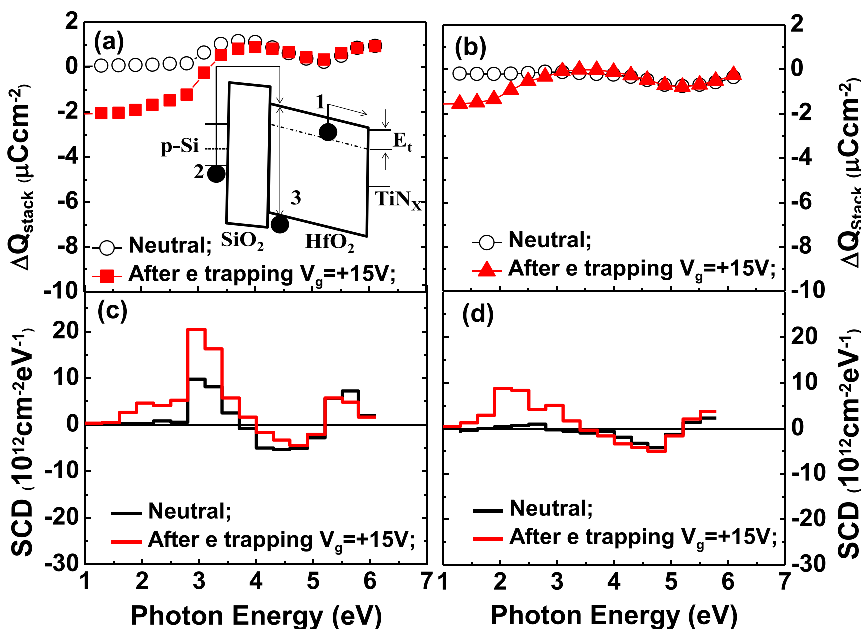

FIG. 1. Illumination-induced charge variations observed under +1 V bias on metal electrode (a), (b) and the inferred SCD distributions (c), (d) for samples with 19-nm thick HfO_2 (a), (c) or $Hf_{0.8}Al_{0.2}O_x$ (b), (d) insulators. Results are shown for both the as-fabricated neutral samples (○) and for the samples injected with electrons by tunneling out of silicon (red online). The inset illustrates the schematics of electron transitions during the EPDS experiment: photoionization of traps with energy E_t (1), electron photoinjection from Si followed by trapping in HfO_2 (2), and electron-hole pair generation in HfO_2 (3).

Reuse of AIP Publishing content is subject to the terms at: https://publishing.aip.org/authors/rights-and-permissions. Download to IP: 128.40.8.138 On: Tue, 31 May 2016 17:14:45

stack, we conclude that there is neither present a detectable density of hole traps nor donor-type gap states in the HfO_2 or $Hf_{0.8}Al_{0.2}O_x$ layers.

Since the excitation of electrons from the gap states into the HfO_2 CB represents the dominant (dis)-charging mechanism in the range $h\nu < 4$ eV, the SCD directly reflects the energy distribution of the initial electron states. The spectral plots in Fig. 1 show that there are at least two main components in the trapped electron density—one shallow ($2\,eV < E_t < 3\,eV$) found both in HfO_2 and $Hf_{0.8}Al_{0.2}O_x$ layers and a deeper one ($3\,eV < E_t < 3.5\,eV$) present in HfO_2. Furthermore, comparison of the SCD distributions observed in ALD HfO_2 layers grown from different precursors (processes A-C), as shown in Fig. 2, panels (a)–(c), respectively, reveals a much lower density of the deep electron traps in the Cl-free sample B while in the sample C (also Cl-free) the shallow traps become dominant. The observation of shallow traps both in the carbon-free HfO_2 films (process A) and in the Cl-free layers grown using metallo-organic precursors (processes B and C) suggests that these defects are not impurity-related, but likely intrinsic.

To get further insight into the origin of the electron traps in HfO_2, we analyzed the effect of annealing on the samples A and C, which exhibit different energy distributions of trapped electrons in the as-deposited state. Figures 3 and 4 show the SCD spectra obtained on the samples A and C, respectively, after 15 min anneal in N_2 at the indicated temperature. In sample type A, the dominant deep traps at around $E_t = 3$ eV

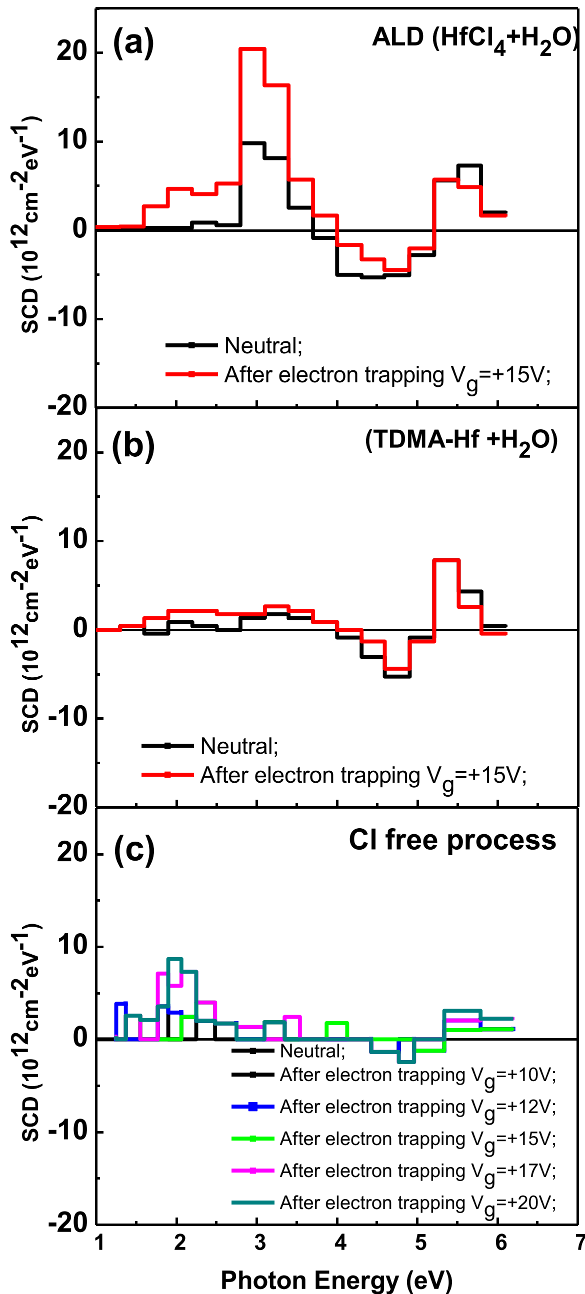

FIG. 2. SCD spectra measured on $Si/SiO_2/HfO_2/Au$ samples with HfO_2 layers deposited using different ALD processes: A, B, C–corresponding panels (a)–(c), respectively.

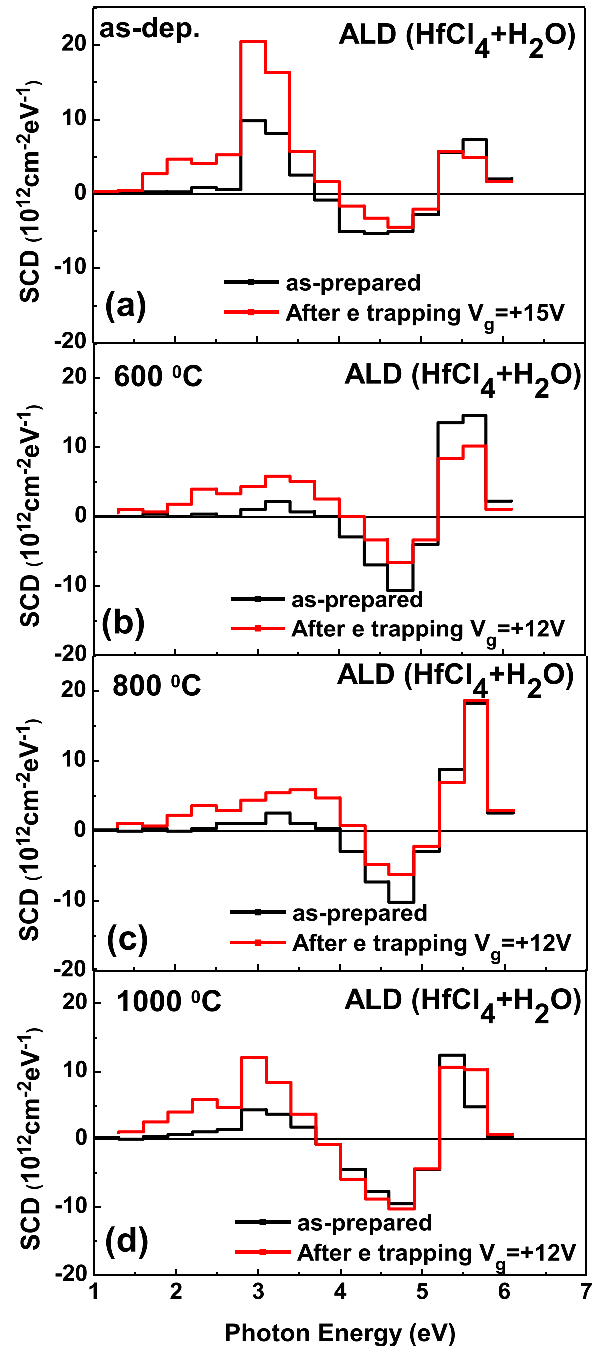

FIG. 3. SCD spectra as measured on $Si/SiO_2/HfO_2$ samples with HfO_2 layers deposited using the ALD process A and subjected to post-deposition 15 min annealing in N_2 at the indicated temperature.

Reuse of AIP Publishing content is subject to the terms at: https://publishing.aip.org/authors/rights-and-permissions. Download to IP: 128.40.8.138 On: Tue, 31 May 2016 17:14:45

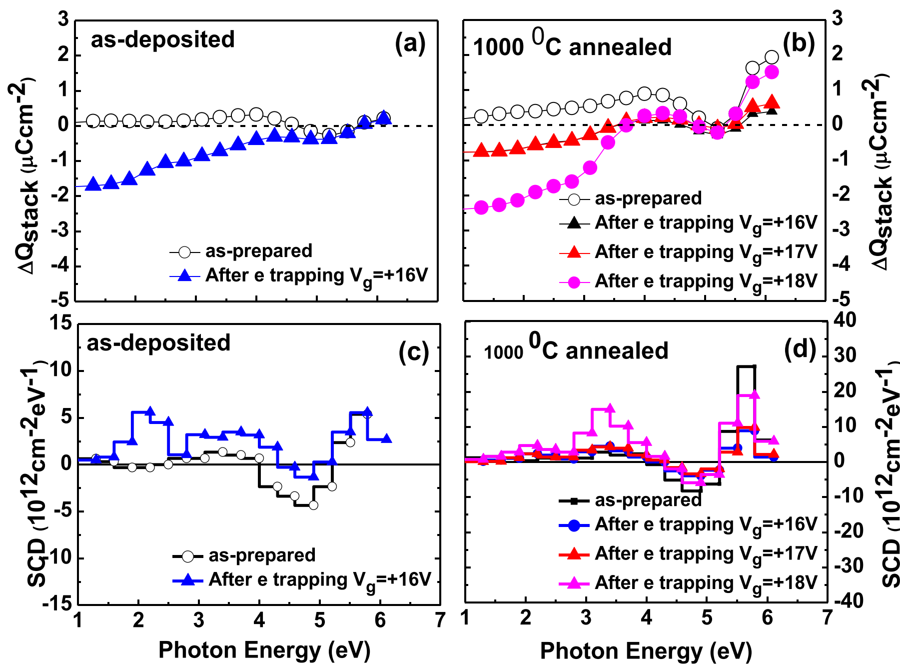

FIG. 4. Illumination-induced charge variation (a), (b) and the inferred SCD spectra (c), (d) as measured on Si/SiO_2/HfO_2 samples with HfO_2 layers deposited using the ALD process C and subjected to post-deposition 15 min annealing in N_2 at 1000 °C. The results of measurements on the electron-injected samples are shown for several charging voltage pulse amplitudes.

(Fig. 3, panel (a)) disappear upon annealing at 600 °C (panel (b)) and 800 °C (panel (c)) but do come back after the anneal at the highest temperature of 1000 °C (d). We also note that the density of positive charge accumulated in the stack upon electron-hole pair generation in HfO_2 ($h\nu > 5.6$ eV) significantly increases as compared to the as-deposited film. The same trends are seen even more clearly in sample type C (cf. Fig. 4) where both the generation of deep electron traps, which are nearly absent in the as-deposited film, and the additional hole trapping leading to the accumulation of net positive charge are observed after heating to 1000 °C. This led us to the hypothesis that the high-temperature (1000 °C) anneal of HfO_2 in the O-free (N_2) ambient may induce oxygen deficiency, prompting us to re-address the O vacancy model.

Since the as-deposited samples are partially crystallized (HfO_2, process A) or amorphous ($Hf_{0.8}Al_{0.2}O_x$, process A), while crystallization with a significant content of the monoclinic (m-) phase is achieved upon annealing, we consider the O vacancy energy levels both in m-HfO_2 and in a-HfO_2. Extensive theoretical studies of the O vacancy in m-HfO_2[17–19] demonstrated that it is a deep hole trap resulting in the +1 or +2 charged states while the electron trapping by the neutral vacancy is expected to occur at a level positioned at ≈1 eV below the m-HfO_2 CB bottom. The calculated energy positions of electron and hole trapping levels are less reliable in a-HfO_2 because of severe underestimation of the bandgap[20,21] suggesting to revisit this issue by performing additional *ab initio* simulations of the a-HfO_2 network with O vacancies included using a non-local density functional.

The details of the calculations can be found in the supplementary material.[27] The obtained a-HfO_2 structures have a density of 9.6 g/cm^3 in good agreement with the experiment. Around 56% of the Hf atoms are bonded to 6 oxygen atoms, 38% are bonded to 7, and 6% to 5 oxygen atoms. On the other hand, 72% of oxygen atoms are bonded to 3 Hf atoms, 22% to 4, and 6% are bonded to 2 Hf atoms. These results are in good agreement with those of other theoretical studies[29,30] and, importantly, do not depend significantly on the force-field used. The oxide bandgap width is close to 6 eV, to be compared to the 5.9 eV experimental values for a-HfO_2[31] or a-$HfAlO_x$.[32] Twenty five oxygen vacancies were created in the fully relaxed a-HfO_2 structure by randomly removing O atoms in accordance with the distribution of the number of nearest neighbour Hf ions described above. The structural relaxation and electronic structures were calculated for positively, neutral, and negatively charged states of these vacancies. The vacancy formation energies as a function of the electron chemical potential are plotted in Fig. 5 with the distribution of formation energies for each coordination number for neutral vacancies shown in an inset. Similar distributions were obtained for charged vacancies. These formation energies vary within about 1.5 eV due to the difference in the local environment and resulting relaxation of the amorphous structure, in good agreement with Ref. 21. The spread of the distribution of all formation energies is used in plotting "bands" in Fig. 5, which substitute lines in similar

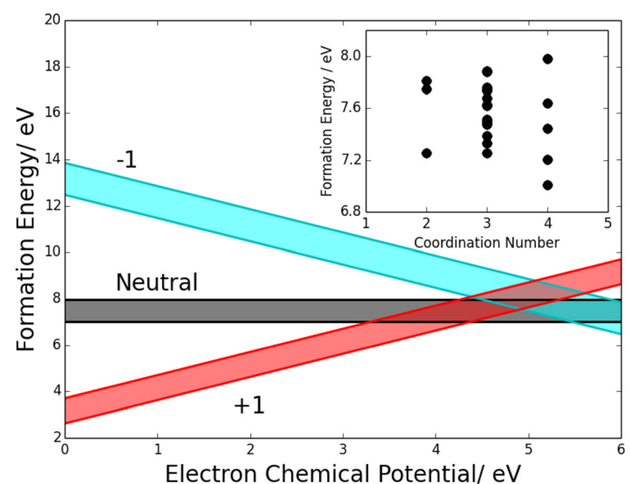

FIG. 5. Calculated formation energies of the singular O vacancy as a function of the electron chemical potential in a-HfO_2, with the origin corresponding to the VB maximum. Charge states are indicated next to the line plots and the width of the line corresponds to the span of formations energies. The inset shows the distribution of formation energies of vacancies as a function of the number of the nearest neighbour Hf ions.

Reuse of AIP Publishing content is subject to the terms at: https://publishing.aip.org/authors/rights-and-permissions. Download to IP: 128.40.8.138 On: Tue, 31 May 2016 17:14:45

plots for crystals. By using the full width of the distribution shown in the inset of Fig. 5, we assume that the vacancies are created in these sites with equal probability. In thermal equilibrium, vacancies will occupy sites with the lowest formation energies and the distribution will be narrower.

As one can see in Fig. 5, the +/0 charge transition levels are located far from the VB top meaning that the formation of the positively charged vacancy by hole trapping from the a-HfO_2 VB would require a multi-phonon process. Nevertheless, these positively charged states can be formed in the vicinity of an electrode and may account for the interface barrier lowering caused by oxygen scavenging from HfO_2 by metallic Hf.[33] On the other hand, the 0/− levels are too shallow to explain the 2-and 3-eV deep states of the trapped electrons distribution. Thus, even after introducing the effect of disorder, the O-vacancy trapping cannot explain the experimental observations mandating the search for alternative models.

The key experimental observation in this study concerns the demonstration of the vast dominance of acceptor states in all studied HfO_2 samples. This abundance of deep acceptors is consistent with the literature reports[34,35] on p-type conductivity of O-deficient HfO_2 though in our study the pristine ALD-grown films are stoichiometric within the accuracy of our measurements. Taking into account that the 2- and 3-eV deep acceptors found in HfO_2 cannot be correlated with the presence of typical precursor residuals (C, Cl), they are most likely related to intrinsic defects in the oxide network. Therefore, one can consider two types of candidate sites for the electron trapping: First, some form of O deficiency, different from the commonly assumed isolated O vacancy, may give rise to electron trapping. Clustering of vacancies[35] or their interaction with hydrogen, as recently revealed in the case of a-SiO_2,[36] represent feasible models deserving further theoretical and experimental analysis. Second, self-trapping of electrons on oxide network sites under strained bonding geometries may also provide deep acceptor states in the amorphous phases[37] or inside the grain boundary region in polycrystalline HfO_2. Considerable site-to-site variations in the trapping geometry expected in this case may explain the relatively wide energy distributions of the trapped electrons as well as the mentioned failure of ESR to detect the corresponding paramagnetic state because of excessive line broadening.

In conclusion, the presented EPDS methodology allows for determination of the energy distribution of electron traps across the entire HfO_2 bandgap. Using this technique, we found two kinds of deep electron traps in ALD-grown HfO_2 energetically distributed at around $E_t \approx 2.0\,eV$ and $E_t \approx 3.0\,eV$ below the oxide CB bottom. Comparison of the trapped electron energy distributions in HfO_2 layers prepared using different Hf precursors or subjected to post-deposition annealing suggests these centers to be intrinsic in nature. However, the hypothesis of the isolated O vacancy being at the origin cannot explain the charging behavior of a- or m-HfO_2, pointing to the need of alternative defect models.

J.S. and A.L.S. are grateful to EPSRC (Grant No. EP/K01739X/1) and EU FP7 project MORDRED (EU Project Grant No. 261868) for financial support and thank the UK's HPC Materials Chemistry Consortium funded by EPSRC (EP/L000202) for providing computer resources on the UK's national high-performance computing service ARCHER. The work at KULeuven has received support from the EU FP7 project MORDRED and from the Fonds Wetenschappelijk Onderzoek-Vlaanderen (Project No. G.0C05.13). A.S. and V.A. also acknowledge the support from the EU COST Action CM1104 "Reducible oxides."

[1] R. D. Clark, Materials **7**, 2913 (2014).
[2] J. Robertson and R. M. Wallace, Mater. Sci. Eng., R **88**, 1 (2015).
[3] G. Molas, M. Bocquet, E. Vianello, L. Perinola, H. Grampeix, J. P. Colonna, L. Masarotto, F. Martin, P. Brainceau, M. Gely, C. Bongiorno, S. Lombardo, G. Pananakakis, G. Gibaudo, and B. De Salvo, Microelectron. Eng. **86**, 1796 (2009).
[4] L. Breuil, J. G. Lisoni, P. Blomme, G. Van den Bosch, and J. Van Houdt, IEEE Electron Device Lett. **35**, 45 (2014).
[5] M. H. Park, Y. H. Lee, H. J. Kim, Y. J. Kim, T. Moon, K. Do Kim, J. Muller, A. Kersch, U. Schroeder, T. Mikolajick, and C. S. Hwang, Adv. Mater. **27**, 1811 (2015).
[6] T. S. Boscke, J. Muller, D. Brauhaus, U. Schroeder, and U. Bottiger, Appl. Phys. Lett. **99**, 102903 (2011).
[7] P. Polakowski and J. Muller, Appl. Phys. Lett. **106**, 232905 (2015).
[8] J. Muller, P. Polakowski, S. Mueller, and T. Mikolajick, ECS J. Solid State Sci. Technol. **4**, N30 (2015).
[9] K. Karda, A. Jain, C. Mouli, and M. A. Alam, Appl. Phys. Lett. **106**, 163501 (2015).
[10] A. Kerber and E. A. Cartier, IEEE Trans. Device Mater. Reliab. **9**, 147 (2009).
[11] E. Cartier, A. Kerber, T. Ando, M. M. Frank, K. Choi, S. Krishnan, B. Linder, K. Zhao, F. Monsieur, J. Stathis, and V. Narayanan, IEEE Int. Electron Devices Meet., Tech. Dig. **2011**, 441.
[12] T. Ando, Materials **5**, 478 (2012).
[13] D. P. Ioannou, Microelectron. Reliab. **54**, 1489 (2014).
[14] B. Govoreanu, R. Degraeve, M. B. Zahid, L. Nyns, M. Cho, B. Kaczer, M. Jurczak, J. A. Kittl, and J. Van Houdt, Microelectron. Eng. **86**, 1807 (2009).
[15] M. B. Zahid, R. Degraeve, L. Breuil, P. Blomme, J. G. Lisoni, G. Van den Bosch, J. Van Houdt, and B. J. Tang, in *International Reliability Physics Symposium, 2014*, p. 2E.3.
[16] J. Muller, P. Polakowski, S. Mueller, and T. Mikolajick, ECS Trans. **64**(8), 159 (2014).
[17] K. Xiong, J. Robertson, M. C. Gibson, and S. J. Clark, Appl. Phys. Lett. **87**, 183505 (2005).
[18] P. Broqvist and A. Pasquarello, Appl. Phys. Lett. **89**, 262904 (2006).
[19] D. Muños Ramo, J. L. Gavartin, A. L. Shluger, and G. Bersuker, Phys. Rev. B **75**, 205336 (2007).
[20] C. Kaneta and T. Yamasaki, Microelectron. Eng. **84**, 2370 (2007).
[21] C. Tang and R. Ramprasad, Phys. Rev. B **81**, 161201 (2010).
[22] V. V. Afanas'ev and A. Stesmans, J. Appl. Phys. **95**, 2518 (2004).
[23] A. Stesmans, V. V. Afanas'ev, F. Chen, and S. A. Campbell, Appl. Phys. Lett. **84**, 4574 (2004).
[24] V. V. Afanas'ev and A. Stesmans, Phys. Rev. B **59**, 2025 (1999).
[25] W. C. Wang, M. Badylevich, V. V. Afanas'ev, A. Stesmans, C. Adelmann, S. Van Elshocht, J. A. Kittl, M. Lukosius, Ch. Walczyk, and Ch. Wenger, Appl. Phys. Lett. **95**, 132903 (2009).
[26] V. V. Afanas'ev, W. C. Wang, F. Cerbu, O. Madia, M. Houssa, and A. Stesmans, ESC Trans. **64**(8), 17 (2014).
[27] See supplementary material at http://dx.doi.org/10.1063/1.4952718 for details of measurement procedure and calculations.
[28] E. E. Hoppe and C. R. Aita, Appl. Phys. Lett. **92**, 141912 (2008).
[29] S. Plimpton, J. Comput. Phys. **117**, 1 (1995).
[30] D. Vanderbilt, X. Zhao, and D. Ceresoli, Thin Solid Films **486**, 125 (2005).
[31] V. V. Afanas'ev, A. Stesmans, F. Chen, X. Shi, and S. A. Campbell, Appl. Phys. Lett. **81**, 1053 (2002).
[32] V. V. Afanas'ev, A. Stesmans, and W. Tsai, Appl. Phys. Lett. **82**, 245 (2003).
[33] V. V. Afanas'ev, A. Stesmans, L. Pantisano, S. Cimino, C. Adelmann, L. Goux, Y. Y. Chen, J. A. Kittl, D. Wouters, and M. Jurczak, Appl. Phys. Lett. **98**, 132901 (2011).
[34] N. Hadacek, A. Nosov, L. Ranno, P. Strobel, and R.-M. Galera, J. Phys.: Condens. Matter **19**, 486206 (2007).
[35] E. Hildebrandt, J. Kurian, M. M. Muller, T. Schroeder, H.-J. Kleebe, and L. Alf, Appl. Phys. Lett. **99**, 112902 (2011).
[36] A. M. El-Sayed, Y. Wimmer, W. Goes, T. Grasser, V. V. Afanas'ev, and A. L. Shluger, Phys. Rev. B **92**, 014107 (2015).
[37] A. M. El-Sayed, M. B. Watkins, V. V. Afanas'ev, and A. L. Shluger, Phys. Rev. B **89**, 125201 (2014).

Reuse of AIP Publishing content is subject to the terms at: https://publishing.aip.org/authors/rights-and-permissions. Download to IP: 128.40.8.138 On: Tue, 31 May 2016 17:14:45